Journal of Materials Chemistry C

ROYAL SOCIETY OF CHEMISTRY

PAPER

View Article Online
View Journal | View Issue

Cite this: J. Mater. Chem. C, 2022, 10, 13930

Smart textiles for human–machine interface fabricated *via* a facile on-site vapor-phase polymerization†

Haoyu Wang,‡[a] Yi Xing,‡[a] Zuo Xiao,[b] Hengda Sun,[a] Gang Wang *[a] and Meifang Zhu[a]

Conducting polymers are widely employed in wearable sensing devices. Their unique compliance and flexibility endow higher tolerance to signal aberrations caused by mechanical mismatch compared to their rigid counterparts. Mostly, wearable sensing devices composed of organic electronic materials are fabricated on smooth-treated substrates and by utilizing complex assembly processes to ensure working validity. Thus, the direct surface functionalization of textiles places a high demand for the integration of the sensing structure. The conventional surface functionalization strategies, such as dip-coating or printing, suffer from large-scale roughness as displayed by the densely woven structure and poor wettability in some textiles, and exhibit inhomogeneity and weak mechanical–electrical stability. Herein, a facile vapor-phase polymerization (VPP) strategy for a highly conductive PEDOT:Tos coating was demonstrated for the direct surface functionalization of various yarns and fabrics, enabling the *in situ* fabrication of electronic textiles while allowing maintaining the inherent advantages of textiles, such as flexibility and mechanical stability. We successfully fabricated strain sensors and three-dimensional (3D) fabric switches by depositing PEDOT:Tos on the surfaces of commercial yarns and fabrics, respectively. The fabricated devices exhibited excellent conductivity, uniformity (linear resistance with length), and impressive mechanical–electrical stability. Further, we constructed human–machine communication interfaces based on electronic yarns and 3D fabrics, and explored their applications in tactile sensing, fabric electronic switches for smart homes and fabric computing.

Received 20th April 2022,
Accepted 8th June 2022

DOI: 10.1039/d2tc01618d

rsc.li/materials-c

Introduction

The rapid development of new artificial intelligence technology in recent years has aroused enthusiasm for research into body-conformable electronic devices. Various flexible electronic devices, such as transducers,[1,2] sensors,[3–5] light-emitting devices,[6,7] and stretchable electronic circuits[8,9] have been integrated into fabrics, enriching the field of wearable electronics. In particular, wearable sensors that act as a communication interface between living organisms and external machines while realizing data collection, information transmission, and interaction are highly demanded.[10] Compared with traditional hand-held devices, wearable sensors provide a novel, convenient, and comfortable way to detect human movement and transmit physiological signals.[11,12] To be incorporated into wearable and flexible electronics, sufficient strength, flexibility, and adhesion are important considerations in material selection. Currently, the strategy of compounding active objects, such as high conductive carbons (graphene, carbon nanotubes (CNTs), carbon blacks (CBs), *etc.*),[13–15] conductive polymers (poly(3,4-ethylenedioxythiophene) (PEDOT), polypyrrole (Ppy), *etc.*),[16,17] and liquid alloys[18] with dielectric plastics (*e.g.*, Ecoflex, perfluoroalkoxy alkane(PFA))[19,20] and rubbers (*e.g.*, polydimethylsiloxane (PDMS)),[21] to meet the requirements of lightweight, sensitive, and durable wearable devices has become popular. At the same time, various fabrication processes can be effectively utilized to fabricate flexible sensors, among which casting, coating, spinning, and transfer have become proven methods in the field.[22–24]

Compared to constructing thin films on flat or rigid substrates, textile-based structure–function-integrated device design can mitigate signal anomalies due to excellent mechanical adaptation while maintaining breathability and

[a] State Key Laboratory for Modification of Chemical Fibers and Polymer Materials, College of Materials Science and Engineering, Shanghai Key Laboratory of Lightweight Structural Composites, Key Laboratory of High Performance Fibers & Products, Ministry of Education, Donghua University, Shanghai 201620, P. R. China. E-mail: gwf8707@dhu.edu.cn

[b] School of Information Science and Technology, Donghua University (DHU), China

† Electronic supplementary information (ESI) available. See DOI: https://doi.org/10.1039/d2tc01618d

‡ These authors contributed equally to this work.

comfortability.[25] However, constructing uniform film sensing devices on fabrics or yarns is considered a dauting task due to the void structure, surface roughness, and unstable topologies. As a classic conducting polymer, PEDOT has tunable conductivity, flexibility, and even sufficient stretchability when fabricated correctly through proper composition techniques.[26–28] Importantly, its loading on substrates can be achieved without complicated processes, compared to silver nanowires and single-walled carbon nanotube dispersions.[29] Recently, PEDOT and its derivatives were loaded on textiles to create wearable conductive primitives.[30,31]

The deposition method significantly affects the physical and chemical properties of electronic textiles.[25] According to the different deposition methods, the final prepared PEDOT composition will be also slightly different, which is reflected in the choice of doping anions.[32] With the presence of poly(styrene sulfonate) (PSS), poly(3,4-ethylenedioxythiophene)-poly(styrene sulfonate) (PEDOT:PSS) exists in an aqueous processable state,[33] making the liquid-phase deposition technique the first choice. Researchers reported dip-coating PEDOT:PSS on natural and man-made fabric substrates.[34,35] Various methods of spraying and printing conductive PEDOT:PSS coatings have also been widely reported.[36,37] Even though PEDOT:PSS is the most commonly used PEDOT composite system in the preparation of flexible conductive devices, PEDOT:PSS is very sensitive to humidity and shows a tendency to swell in aqueous media due to the water-soluble PSS chains.[38] Besides the effect of aqueous solution, the weak adhesion of polymers to textiles is another reason for the deterioration of a textile's properties.[32,39] Some additives have been used to improve the adhesion between PEDOT:PSS and fabrics, but most of these additives are insulating and can negatively affect the breathability and comfort of the fabrics.[40]

Vapor-phase polymerization (VPP) is an effective technique to uniformly deposit PEDOT coatings on target substrates. By adjusting parameters such as the temperature, air pressure, and humidity, the surface of a PEDOT coating can retain the original texture of the matrix textiles, such as woven and mesh structures.[41,42] The preservation of this fine structure is essential for maintaining the current path and provides a smoother energy environment for carrier transport of fabric-based sensors. Further, the VPP method enables the development of water-repellent PEDOT coatings, so that the fabricated sensor devices can maintain long-term operation in a high-humidity environment.[38]

In this work, the initial conductivity of VPP poly(3,4 ethylenedioxythiophene)-tosylate (PEDOT:Tos) (abbreviated as VPP PEDOT) films was enhanced by doping the active species polyethylene glycol (PEG) in an oxidant solution. The loading of uniform VPP PEDOT conductive coatings on commonly used commercial yarns (nylon, cotton, fiberglass, polyurethane (PU)) and fabrics (polyethylene glycol terephthalate (PET), cotton, nylon, and viscose) was achieved through a spontaneous drying process of the oxidant without any binder and a subsequent doping treatment, verifying the versatility of VPP for the surface modification of VPP PEDOT on various textile surfaces. The prepared electronic yarn exhibited high sensitivity and reproductivity for the motion signal tracking of human joints. We fabricated a switch-type resistive sensor by on-site constructing PEDOT on the surface of a 3D spacer fabric, exhibiting good performance stability during a 150 times cyclic pressing process. We further constructed a human–machine interface based on 3D spacer fabric switches and explored their applications in fabric electronic switches for smart homes and fabric computing to demonstrate the practicality of the VPP PEDOT coating as an interactive sensor.

Gang Wang

Gang Wang has been a full professor at the State Key Lab for Modification of Chemical Fibers and Polymer Materials (SKLFPM), Donghua University, since November 2019. Before that, he carried out research at the Georgia Institute of Technology and Northwestern University from 2013 to 2019. He obtained his PhD degree in Materials Science and Engineering from Donghua University, China. His current research interests include electronic (especially semiconducting) fibers and smart clothing for human–machine interfaces. He has published over 60 peer-reviewed articles, including in Nature Materials, PNAS, and JACS. Currently, he also serves as an academic editor for Advanced Fiber Materials.

Experimental

Materials

3,4-Ethylenedioxythiophene (EDOT, >99%) was purchased from Rhawn Chemical Technology Co., Ltd. PEDOT:PSS (Clevios® PH 1000) was purchased from Heraeus. Iron(iii) *p*-toluenesulfonate hexahydrate ($Fe(Tos)_3$, 98%) and 1-butanol (AR, 99%) were received from Shanghai Macklin Biochemical Co., Ltd. Pyridine (safe dry, with molecular sieves, 99.5%) was obtained from Adamas. PEG (AR, M_w = 200) was purchased from Sinopharm Chemical Reagent Co., Ltd. All the chemicals were used without further purification. Nylon spacer fabric, spandex yarns, nylon yarns, fiberglass yarns, and cotton yarns were received from Donghua University College of Textiles.

Preparation of PEDOT thin films

PEDOT:Tos films were prepared by a vapor-phase polymerization (VPP) of EDOT monomers within a vacuum heating desiccator (Selecta®), specifically by fixing the amount of $Fe(Tos)_3$ and pyridine to 2 g and 0.2 g, adding PEG with a mass fraction of 0–12%, and finally dissolving them to 5 g with 1-butanol as the oxidant solution. The oxidizer solution was spin-coated onto pre-cleaned 2.5 × 2.5 cm glass substrates at

1000 rpm for 30 s. After 2 min of heating on a hotplate at 70 °C, the samples were placed into the desiccator. EDOT droplets were drop-cast on the glass substrates inside the 70 °C chamber in a way to ensure that the monomer vapor could reach the samples surface unhindered. The vacuum valve was turned off after pumping down the desiccator to −76 cmHg. During the polymerization in 30 min, the surfaces of the samples could be observed to gradually change from yellow to blue-green. After the polymerization, the chamber was vented and the samples were taken out and immersed in an ethanol bath. The PEDOT:Tos films rapidly turned light blue by applying small-amplitude mechanical perturbations to the ethanol. After the above process, all the samples were nitrogen dried at room temperature. The film thickness and square resistance used in the calculations were taken from the average of at least three measurements, and the calculated conductivity values were taken from the average of at least six individual samples.

PEDOT:Tos- and PEDOT:PSS-coated electronic yarns and flexible fabrics

The oxidant solutions for preparing the flexible devices consisted of 40 wt% $Fe(Tos)_3$ and 6 wt% PEG in 1-butanol. The yarns and textiles were heated on a hot stage at 70 °C for 2 min, after which the oxidant solutions were sprayed with a spray gun until the surface of the yarns were evenly covered. The samples were then dried for 2 min to volatilize the butanol, and the above process was repeated 2–3 times to obtain highly conformal oxidant-coated textiles and yarns. The $Fe(Tos)_3$-coated textiles or yarns were exposed to EDOT vapor for 30 min in the desiccator mentioned above at 70 °C under vacuum conditions. The resultant PEDOT-coated samples were washed repeatedly with ethanol several times until the surfaces turned from yellow to blue, followed by drying at room temperature for 30 min. The PEDOT:PSS-coated yarns were made by immersing them in a beaker containing an aqueous solution of PEDOT:PSS for 2 h.

Washing and two-dimensional conductivity uniformity tests

The washing test used PET fabrics (2.5 cm × 2.5 cm) loaded with PEDOT:PSS and VPP PEDOT. The fabrics were soaked in deionized water and stirred with a magnet, and then taken out every 1 h and dried in a 70 °C oven. A four-pointer tester was used to test the square resistance of each piece of fabric at six locations. The resistance uniformity test was carried out on a 2.5 cm × 6 cm piece of PET fabric, using silver paste to construct 10, 20, 30, 40, and 50 mm long conductive paths (Fig. S5, ESI†). One end of a Keithley 6500 electrode was fixed in the origin silver paste area and the other end of the electrode used to contact the silver paste a certain length from the origin, staying there for 2 s until a stable reading was displayed. Each data point obtained in this part of the tests reflects the performance of at least six samples.

Fabrication of flexible strain sensors and spacer fabric arrays

In order to avoid baseline fluctuations due to the interface problems as much as possible, copper tape was fixed on both ends of the PEDOT:Tos-loaded yarn through silver paste, and commercial copper wire (PVC-coated tin-plated copper wire, URBEST 305M) was welded on to the copper tape as an extended electrode. UV-curable glue was applied to the solder joints and the yarn was fixed to the nitrile glove, and the two electrodes of a Keithley 6500 system were fixed to two commercial copper wires that extended out. The Keithley 6500 was able to detect changes in the resistance signal due to the bending of fingers. The tensile tester was adjusted to stretch 45% for 1 s, continued for 15 cycles; then with both ends of the yarn clamped by two Keithley 6500 electrodes, the relationship between the tensile strength and the resistance change could be obtained. An ESP-32 circuit board was used to collect the data of the fabric buttons. The specific circuit diagram is shown in Fig. S6, ESI.† Every two adjacent buttons were connected to the same port, and the TXTS0108E step-down chip was used to distribute 3.3 V and 2.1 V voltages to the two buttons.

Characterization

Ultradeep images were captured using an Ultra Depth Microscope (DVM6 LEICA). Here, 100 and 500 magnifications were used in the characterization. The sheet resistance of the film was measured on the film surface *via* the four-point probe method using a 4-point probe resistivity measurement system (RTS-9, Guangzhou Four Probe Technology). The film thickness was measured by a stylus profiler (Dektak XT, Bruker). The conductivity of the film was calculated by $\sigma = 1/(R_{sq} \times \delta)$, where R_{sq} is the sheet resistance of the film and δ is the thickness of the film. An InVia Reflex Raman microscope was used to record the Raman spectra (532 nm excitation). X-Ray photoelectron spectroscopy (XPS) was performed on an Escalab 250Xi system. Scanning electron microscopy (SEM) was performed using a cold field emission-scanning electron microscope (FlexSEM 1000II). Strain-resistance change testing was done by combining INSTRON/5969 and Keithley 6500 systems, with the latter also used in the yarn sensor section.

Results and discussion

Fabrication and microstructure analysis of PEDOT:Tos *via* VPP

A clear advantage of the VPP process is that it allows the scalable preparation of oxidants and thereby enhances the performance relative to pristine films.[43] We prepared VPP PEDOT (chemical structure shown in Fig. 1b) films *via* the VPP method, as illustrated in Fig. 1a. More experimental details are documented in the experimental section. Briefly, the process mainly consisted of four basic stages: (1) drop-casting the oxidant solutions on the substrate; (2) oxidant film formation by spin coating and drying; (3) deposition and polymerization of EDOT on top of the substrates transferred into a desiccator; (4) removal of unreacted iron(III) *p*-toluene sulfonate hexahydrate ($Fe(Tos)_3$) and monomers were *via* ethanol bath washing. Polyethylene glycol (PEG), a biocompatible surfactant reported to improve film conductivity by optimizing film microstructure and chain stacking,[44,45] was added with different weight ratios of 0, 3, 6, and 12 wt%, and labeled as 0-PEDOT, 3-PEDOT,

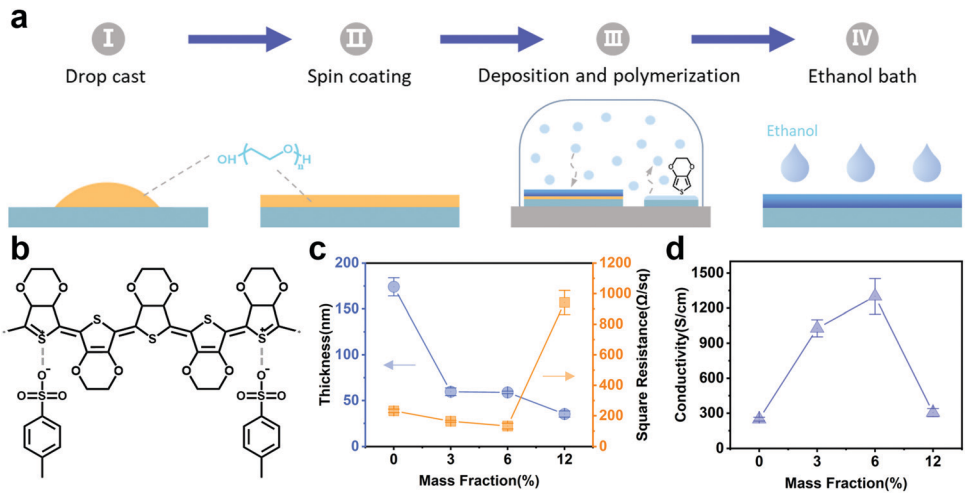

Fig. 1 Synthesis process and conductivity of the VPP PEDOT films. (a) Process flow for the preparing VPP PEDOT film *via* VPP: (I) oxidant dropwise, (II) spin coating, (III) substrate transfer and monomer deposition, (IV) ethanol bath. (b) Chemical structure of VPP PEDOT. (c and d) Thickness and square resistance and conductivity of VPP PEDOT Film with 0, 3, 6, 12 wt% PEG addition.

6-PEDOT, and 12-PEDOT. For the range of PEG contents measured in this study, the thickness of the film decreased from the initial ~174 nm to ~60 nm and then reduced to 35 nm in the subsequent additions, accompanied by a non-linear change in the square resistance (~232 to ~132 Ω sq^{-1} and then a drastic increase to ~942 Ω sq^{-1}) (Fig. 1c), which led to the conductivity initially increasing from ~248 to ~1300 S cm^{-1} and then gradually decreasing to ~304 S cm^{-1} (Fig. 1d). The persistent decrease in film thickness could be attributed to the inhibition of the apparent reactivity of $Fe(Tos)_3$ by PEG *via* metal–ion complexation or steric hindrance, which has a similar effect as the addition of base inhibitors (pyridine, imidazole, *etc.*).[46] We observed that the addition of PEG suppressed the formation of domains in the micrometer range, thereby contributing to the formation of a smooth surface and reducing the barriers in the transport path for carriers (Fig. S1, ESI†). When the PEG content varied by a large amount, it was obvious that there was a trade-off between the addition amount and the conductivity (Fig. 1d).

The curves in Fig. 2a show the Raman spectra of the films with 0, 6, and 12 wt% of PEG added from the bottom to the top. The Raman spectra of the VPP PEDOT films with PEG added were similar to that of the pristine film. The bands between 1400 and 1500 cm^{-1} originated from the $C_\alpha = C_\beta$ (–O) symmetric stretching vibration in the PEDOT neutral structure chains.[47,48] A number of significant changes were revealed in this series of spectra with the addition of PEG increasing. The most significant one was a shift in the symmetric $C_\alpha = C_\beta$ (–O) stretch band, which moved from 1429 cm^{-1} in 0-PEDOT to 1434 cm^{-1} in 12-PEDOT (Fig. 2b). Besides, another noticeable change in this spectrum was the splitting of the band between 1530 to 1590 cm^{-1}. These indicated strong π–π interactions of the aromatic structures of PEDOT after adding PEG. It has previously been reported that the shift of the $C_\alpha = C_\beta$ symmetric stretching vibration band to higher wavenumbers marks an increase in the doping level of PEDOT, which is more dominated by the oxidized structure.[49] Therefore, the addition of PEG is beneficial to improving the doping level to a certain extent. The bands at 1510, 1366, 1267, 1100, 992, 700, and 577 cm^{-1} were assigned to asymmetric $C_\alpha = C_\beta$ stretching, $C_\beta = C_\beta$ stretching, $C_\alpha = C_{\alpha'}$ inter-ring stretching, C–O–C deformation, oxyethylene ring deformation, symmetric C–S–C deformation, and oxyethylene ring deformation.[50] By normalizing the peak at 992 cm^{-1}, the doped states could be compared using

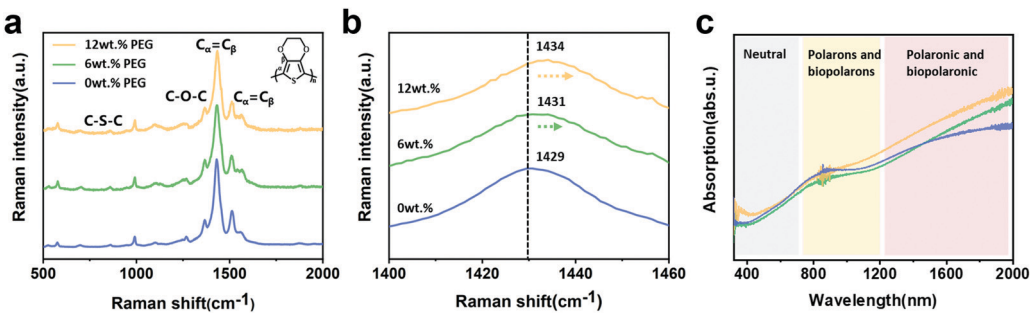

Fig. 2 The microstructure analysis of the VPP PEDOT film fabricated *via* vapor phase polymerization. (a–c) Raman and UV-Vis-NIR spectra of PEDOT film with 0, 6, 12 wt% PEG additions, where (b) is an enlarged image of the Raman spectra near the symmetric $C_\alpha = C_\beta$ (–O) stretch absorption band.

the peak intensities at 1366 and 1429 cm^{-1}, which reflected the benzylic structure of PEDOT chain.[51] More benzylic structures appeared in 0-PEDOT, indicating a lower degree of doping (Fig. S2, ESI†). The UV-Vis-NIR absorption spectra of the PEDOT thin films prepared using different amounts of PEG in the wavelength range of 300 to 2000 nm are presented in Fig. 2c (normalized thickness). With the addition of PEG, the absorption of the PEDOT film increased gradually above 1200 nm and the intensity of the broad signal at 900–1000 nm was reduced, which indicated the polaron energy level gradually changed to the bipolaron state and the oxidation level of PEDOT increased.[52,53] We observed that the Raman and UV-Vis-NIR spectra of 12-PEDOT showed information that did not match the film conductivity. According to the research by Fabretto *et al.*,[46] the substantial increase of the square resistance and reduction in conductivity at high PEG loading should be due to the steric hindrance of the surfactant acting to insulate individual PEDOT grains.

PEDOT-based electronic yarns and fabrics

Surface-modified commercial fabrics of VPP PEDOT for simple wearable sensors have been reported.[54–56] Here, we constructed uniformly covered conductive VPP PEDOT coatings on commonly used yarns *via* a simple oxidant drying–film-forming process. In order to verify that VPP can form uniform PEDOT film on various hydrophobic surfaces compared to the dip-coating treatment method, VPP PEDOT as well as dip-coated PEDOT:PSS were applied to the surface of four yarns (cotton, PU, nylon, fiberglass) and fabrics (cotton, PET, nylon, viscose). As shown in Fig. 3 and Fig. S3 in the ESI,† the VPP process successfully achieved a uniform film coverage on all substrates, while the yarns substrates after dip-coating PEDOT:PSS for 2 h showed a poor adhesion between the surfaces and the coatings. All the yarns were observed by ultradeep microscopy to achieve continuous VPP PEDOT coatings at large scales (Fig. 3a). Fig. 3b shows the scanning electron microscopy (SEM) imagines of these yarns. The EDS image (Fig. S4, ESI†) showed that the surface of the washed yarn exhibited a very low Fe content, and the enrichment of S showed that PEDOT:Tos had been deposited on the substrate. Compared with the original unpolymerized sample (Fig. 3b), the PEDOT coating uniformly wrapped the curved surface of different yarns and exhibited a typical cohesive deposition structure on the surface of the PU and cotton yarn, which was formed by the overlapping of the oxidants between individual fibers under the action of surface tension. This bridging structure caused by the oxidant film tends to lead the VPP process to form a different surface topography on the substrate than the oxidative chemical vapor deposition (oCVD) method.[39,57] We assumed that the film of the oxidant on the surface of the yarn with a dense and braided structure caused the monomers deposited in the early stage of the reaction to act as a shielding layer, hindering the diffusion of the monomers into the yarn, so that the deposition layer tended to form a conformal coating on the single strand rather than a single fiber. Generally, the VPP process appeared to allow PEDOT functionalization of a variety of commonly used yarns. In addition, the PEDOT functionalization of 2D fabrics based on the VPP method also showed satisfactory results, with the four used fabrics possessing different hydrophobicities all exhibiting good adhesion (Fig. 3c). On the contrary, after dip-coating the hydrophobic fabrics represented by nylon and PET, PEDOT:PSS only formed a conductive coating on the surface of the latter one. Yet the resulting fabric tended to be more rigid than the fabrics treated by the VPP process (as illustrated in Fig. 3d and e), which is not preferred for comfortable wearable electronics. A brittle surface is prone to problems such as cracks, resulting in abnormal responses to electrical signals. VPP PEDOT and PEDOT:PSS were used to fabricate conductive coatings on the surface of PET fabrics, and silver paste was used

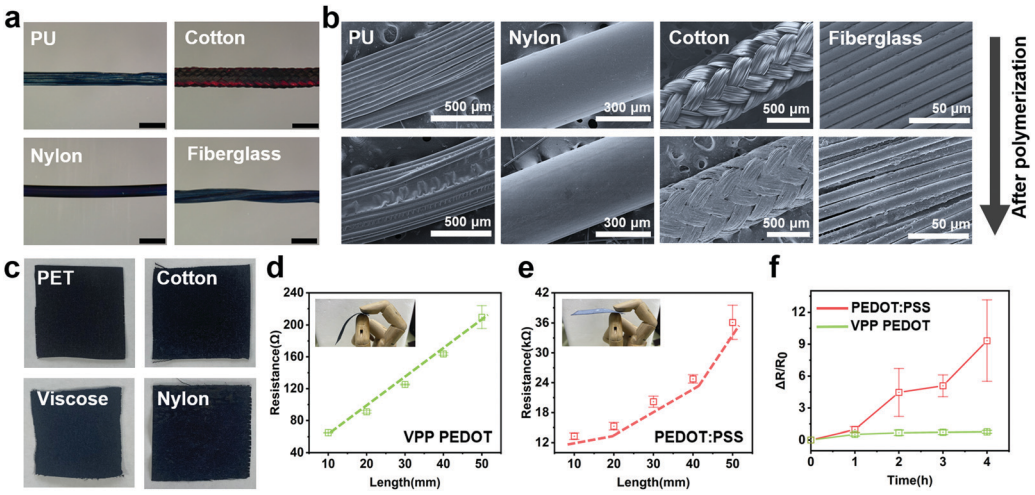

Fig. 3 PEDOT-based electronic textiles fabricated on various substrates. (a) Ultradepth microscope images of the yarns with VPP PEDOT coating, scale bar: 400 μm. (b) SEM images of the yarns with and without VPP PEDOT coating. (c) Photoimages of the fabrics (PET, cotton, viscose and nylon, 2.5 cm × 2.5 cm) coated by VPP PEDOT. (d and e) Constructing channels of increasing length on VPP PEDOT and PEDOT:PSS dip-coated PET fabrics using silver paste to test the uniformity of resistance as a function of distance. Inset shows the flexibility of the PEDOT:PSS- as well as VPP PEDOT-coated PET fabrics. (f) Washing resistance of the VPP PEDOT -and PEDOT:PSS-dip-coated PET fabrics.

to define conductive channels of different lengths to study the two-dimensional conductivity uniformity of the PEDOT coatings prepared by the two methods. The length of the channel was between 10–50 mm, as shown in Fig. S5, ESI.† The channel resistance of the VPP PEDOT coating exhibited an obvious linear relationship with the length, indicating that the thin film followed the standard Ohm's law for the definition between the length and resistance of a single homogeneous conductor (Fig. 3d); while relationship between the channel length and resistance of the PEDOT:PSS coating was rather nonlinear, indicating the difficulty for PEDOT:PSS to form homogeneous conductive paths on fabric substrates (Fig. 3e). Further, to confirm the washability of the VPP PEDOT coating, we placed the PET fabrics loaded with VPP PEDOT and PEDOT:PSS in a beaker filled with deionized water, continuously stirred with a magnet, and measured the square resistance periodically. The results showed that the square resistance of the PEDOT:PSS coating increased dramatically to tenfold, while the resistance of VPP PEDOT showed only a slight increase during the washing process in 4 h (Fig. 3f). The phenomenon indicated that the PEDOT:PSS was able to be desorbed from the fabric during the washing. Therefore, the VPP-treated textiles exhibit higher mechanical strength and durability under laundering treatment. This compatibility with all types of textiles and adhesion stability are essential to ensure the long-term operation of wearable sensor devices and the ability to resist wear and tear from complex physical activities.

PEDOT-based electronic textiles for human–machine interfaces

Flexible PEDOT-based electronic textiles strain sensors can also be used to sense more complex body movements, such as finger flexing. The relative change in resistance is defined as $\Delta R/R_0$, where ΔR and R_0 represent the change in resistance and baseline resistance. The high conformability and elongation of the VPP PEDOT-coated PU yarns endowed a wide operating range. Yarns could produce an effective electrical signal response to deformation and maintained cycling stability at 45% strain (Fig. 4a). As shown in Fig. 4b and d, the yarn could distinguish the bending angles of the finger by the clear change of the resistance signal. Besides, the sensors maintained repeatable and accurate resistance signals during continuous flexion and relaxation of the fingers at different amplitudes or durations as shown in Fig. 4c. The fast bending cycle test for 150 times showed no significant resistance degradation and response times could be as low as 0.06 s and 0.18 s.

Strain-gated switch systems have recently been developed for wearable human–machine interfaces.[58] Switch-based fabric active interaction systems must meet people's work needs in the absence of self-contained electronics, such as simple computing, typing, and location recognition. Here, we constructed a PEDOT conductive layer on 3D spacer fabric surface through an on-site VPP process (Fig. 5a). The homogeneous deposition of VPP PEDOT on the uneven surface of 3D nylon fabric was confirmed by micromorphological analysis (Fig. 5b). Here, 3D fabric with VPP PEDOT was deposited on both sides of the 3D spacer fabric separated by an insulating nylon core yarn (Fig. 5c). Digital photos of single spacer fabric key pixels are shown in Fig. 5d. To verify the effectiveness of the switch key, we connected the spacer fabric in series with the light bulb (Fig. 5e). When a certain pressure was applied to the upper surface of the fabric until it touched the lower surface, the circuit was turned on and the bulb was lit (schematic in Fig. 5f).

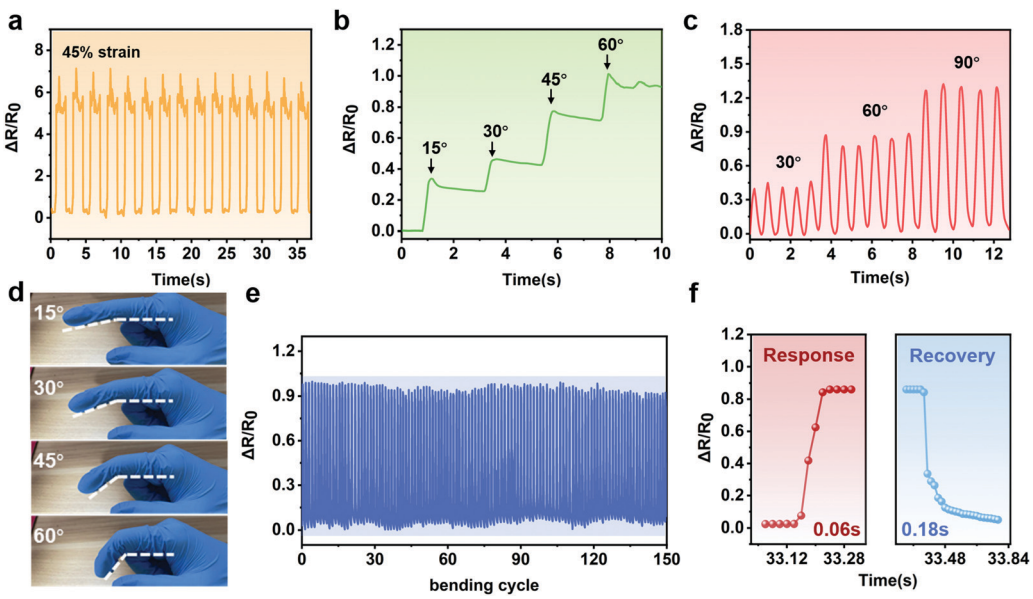

Fig. 4 VPP PEDOT-coated PU yarns for tactile sensors. (a) Resistance response of the VPP PEDOT-coated PU yarns under cyclic loading at 45% strain. (b) Resistive response when fingers were bent and held at different angles. (c) Resistive response of fingers cycled at different bending angles, from top to bottom, of 15°, 30°, 45°, 60°. Tactile sensor affixed to the knuckles (d and e) for a continuous fast bending cycle test for 150 times with the finger held at 60° flexion. (f) Time response in the fast bending cycle test.

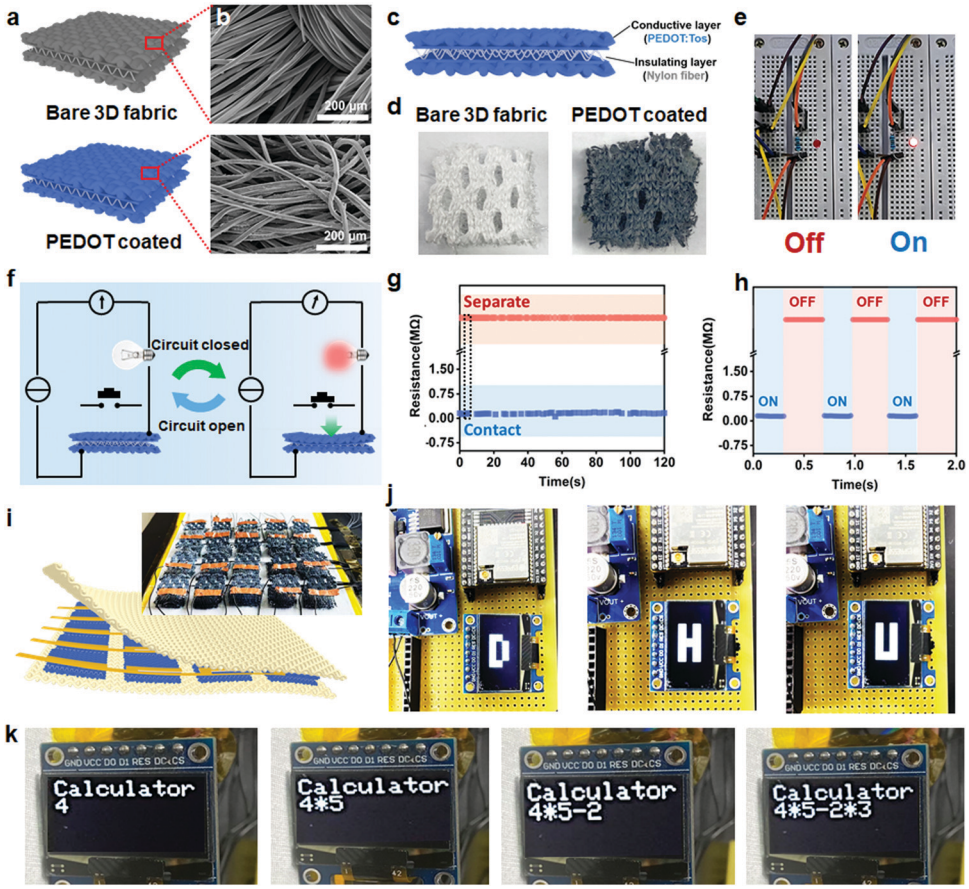

Fig. 5 VPP PEDOT-coated spacer fabric for an electronic switch. (a) Schematic of the VPP PEDOT-coated PET switch fabric: (top) bare 3D fabric with nylon veil; (bottom) 3D fabric after coating PEDOT. (b) SEM images of the 3D fabric before (top) and after (bottom) coating with VPP PEDOT. (c) Single fabric switch pixel. (d) Digital photograph of a fabric switch (2 cm × 2 cm). (e and f) PEDOT-coated 3D fabric connected to an LED bulb to form a series circuit, whereby the bulb lit when the upper and lower sides were in contact due to the action of force. (g) Electrical signal response when fabric switch was repeatedly activated for 150 times within 120 s and (h) with turn-on and turn-off due to the press-release process within 2 s. Enlarged views of the parts in the box: (i) spacer fabric array, (j) spaced fabric arrays for position tracking sensors and (k) fabric computing.

The key maintained stable electrical performance during the 150 times uninterrupted open–close process (within 120 s) and the details of turn-on and turn-off due to the press-release process within 2 s are shown in Fig. 5g and h. No degradation was observed in the electrical properties of the keys during the test, and the entire circuit was able to be quickly disconnected after the force was removed due to the high resilience of the nylon core, which is important for building precise contact–separation and single-shot feedback buttons.

PEDOT-loaded spacer fabric switches were further assembled as key arrays to verify their potential for wearable graphics and computing devices (Fig. 5i). We defined the state of the spacer fabric as the "off" state when it was separated, and when in contact as the "on" state. By assigning different voltage signals to the same port, it was easy to distinguish the position of the array where the fabric switch was located. The fabric switch triggered discernible tactile trajectory tracking with upper and lower electrode contact, with each pair of top and bottom electrodes constituting a sensing pixel. By scanning all the electrode interconnects, the loop channels with voltage output could be identified and the pressed pixels could be accurately identified. Therefore, the images of the three letters D, H, and U could be clearly identified according to the trajectory tracking (Fig. 5j and Movie S1, ESI†). Because of the high sensitivity and flexibility and persistence during the transition between the two states, the fabric switches could act as flexible keyboards for all-fabric input systems. Kickback signal problems that often occur during the use of textile-based progressive keys, such as capacitive or piezoresistive,[59] were not observed during our experiment. As a fabric integrated keyboard device, it could meet the input function without external electronic equipment. Convenient calculations (Fig. 5k) were implemented as a proof-of-concept exhibition. In the longer term, we believe that this precise fabric key could be expected to cooperate with fabric display, fabric storage, and computing fabric devices, thereby promoting the development of wearable all-textile electronic closed loops.

Conclusions

In summary, VPP was demonstrated to serve as a versatile strategy for the direct surface coating of PEDOT on various yarns and fabrics, thus forming portable electronic sensing

textiles. Compared with the conventional dip-coating method using PEDOT:PSS, the VPP method significantly improved the surface adhesion, especially on hydrophobic surfaces. The obtained electronic textiles possessed high water resistance, conductive uniformity/linearity, and robustness, while retaining the original flexibility of the fabric. We further constructed a human–machine interface based on electronic yarns/fabrics and explored their applications in tactile sensors, fabric electronic switches for smart homes, and computational fabrics. The electronic yarn demonstrated the distinct sensing of stretch and the stable, repeatable discrimination of finger bending even under multiple rapid bends. The 3D fabric button had a sensitive control of the circuit on or off state, and the spacing and stiffness of the middle insulating layer prevented the possible short circuit caused by false touches. By integrating these buttons and the corresponding program design, a 3D fabric sensor array with the functions of trajectory tracking and fabric computing was demonstrated. These results exhibit a facile strategy to build electronic textiles for human–machine interfaces, which may have broad application potential, especially in scenarios of health assistance, textile robots, and VR interactions.

Author contributions

H. Y. Wang prepared films, conductive yarns, fabrics and performed electrical and optical characterization; Z. Xiao was responsible for the circuit design of the fabric array; Y. Xing and H. Y. Wang organized the data and wrote the manuscript, G. Wang, M. F. Zhu and H. D. Sun supervised the project; H. Y. Wang and Y. Xing contributed equally to this work. All the authors reviewed and commented on the manuscript.

Conflicts of interest

The authors declare no conflict of interest.

Acknowledgements

We are grateful for the National Natural Science Foundation of China (92163132, 52003049 and 52173156), the Science and Technology Commission of Shanghai Municipality (21520710700, 19JC1410600, 19ZR1470600 and 20JC1414900), the Fundamental Research Funds for the Central Universities (21D110619, 2232021G-02 and 2232021G-12).

Notes and references

1 T. Sun, B. Zhou, Q. Zheng, L. Wang, W. Jiang and G. J. Snyder, *Nat. Commun.*, 2020, **11**, 572.
2 R. Wang, Z. Du, Z. Xia, J. Liu, P. Li, Z. Wu, Y. Yue, Y. Xiang, J. Meng, D. Liu, W. Xu, X. Tao, G. Tao and B. Su, *Adv. Funct. Mater.*, 2022, **32**, 2107682.
3 W. Yan, G. Noel, G. Loke, E. Meiklejohn, T. Khudiyev, J. Marion, G. Rui, J. Lin, J. Cherston, A. Sahasrabudhe, J. Wilbert, I. Wicaksono, R. W. Hoyt, A. Missakian, L. Zhu, C. Ma, J. Joannopoulos and Y. Fink, *Nature*, 2022, **603**, 616–623.
4 R. Liu, J. Li, M. Li, Q. Zhang, G. Shi, Y. Li, C. Hou and H. Wang, *ACS Appl. Mater. Interfaces*, 2020, **12**, 46446–46454.
5 A. Koh, D. Kang, Y. Xue, S. Lee, M. Pielak Rafal, J. Kim, T. Hwang, S. Min, A. Banks, P. Bastien, C. Manco Megan, L. Wang, R. Ammann Kaitlyn, K.-I. Jang, P. Won, S. Han, R. Ghaffari, U. Paik, J. Slepian Marvin, G. Balooch, Y. Huang and A. Rogers John, *Sci. Transl. Med.*, 2016, **8**, 366ra165.
6 X. Shi, Y. Zuo, P. Zhai, J. Shen, Y. Yang, Z. Gao, M. Liao, J. Wu, J. Wang, X. Xu, Q. Tong, B. Zhang, B. Wang, X. Sun, L. Zhang, Q. Pei, D. Jin, P. Chen and H. Peng, *Nature*, 2021, **591**, 240–245.
7 H. W. Choi, D.-W. Shin, J. Yang, S. Lee, C. Figueiredo, S. Sinopoli, K. Ullrich, P. Jovančić, A. Marrani, R. Momentè, J. Gomes, R. Branquinho, U. Emanuele, H. Lee, S. Y. Bang, S.-M. Jung, S. D. Han, S. Zhan, W. Harden-Chaters, Y.-H. Suh, X.-B. Fan, T. H. Lee, M. Chowdhury, Y. Choi, S. Nicotera, A. Torchia, F. M. Moncunill, V. G. Candel, N. Durães, K. Chang, S. Cho, C.-H. Kim, M. Lucassen, A. Nejim, D. Jiménez, M. Springer, Y.-W. Lee, S. Cha, J. I. Sohn, R. Igreja, K. Song, P. Barquinha, R. Martins, G. A. J. Amaratunga, L. G. Occhipinti, M. Chhowalla and J. M. Kim, *Nat. Commun.*, 2022, **13**, 814.
8 Y. Yang, X. Wei, N. Zhang, J. Zheng, X. Chen, Q. Wen, X. Luo, C.-Y. Lee, X. Liu, X. Zhang, J. Chen, C. Tao, W. Zhang and X. Fan, *Nat. Commun.*, 2021, **12**, 4876.
9 I. Wicaksono, C. I. Tucker, T. Sun, C. A. Guerrero, C. Liu, W. M. Woo, E. J. Pence and C. Dagdeviren, *npj Flex. Electron.*, 2020, **4**, 5.
10 Y. Yang and W. Gao, *Chem. Soc. Rev.*, 2019, **48**, 1465–1491.
11 Z. Zhang, L. Cui, X. Shi, X. Tian, D. Wang, C. Gu, E. Chen, X. Cheng, Y. Xu, Y. Hu, J. Zhang, L. Zhou, H. H. Fong, P. Ma, G. Jiang, X. Sun, B. Zhang and H. Peng, *Adv. Mater.*, 2018, **30**, 1800323.
12 M. Amjadi, K.-U. Kyung, I. Park and M. Sitti, *Adv. Funct. Mater.*, 2016, **26**, 1678–1698.
13 G. Cai, M. Yang, J. Pan, D. Cheng, Z. Xia, X. Wang and B. Tang, *ACS Appl. Mater. Interfaces*, 2018, **10**, 32726–32735.
14 Y. Zhao, M. Ren, Y. Shang, J. Li, S. Wang, W. Zhai, G. Zheng, K. Dai, C. Liu and C. Shen, *Compos. Sci. Technol.*, 2020, **200**, 108448.
15 F. Sun, M. Tian, X. Sun, T. Xu, X. Liu, S. Zhu, X. Zhang and L. Qu, *Nano Lett.*, 2019, **19**, 6592–6599.
16 P. Zhao, R. Zhang, Y. Tong, X. Zhao, T. Zhang, Q. Tang and Y. Liu, *ACS Appl. Mater. Interfaces*, 2020, **12**, 55083–55093.
17 H. Cheng, B. Wang, K. Yang, Y. Q. Yang and C. Wang, *Chem. Eng. J.*, 2021, **426**, 131152.
18 Z. Ma, Q. Huang, Q. Xu, Q. Zhuang, X. Zhao, Y. Yang, H. Qiu, Z. Yang, C. Wang, Y. Chai and Z. Zheng, *Nat. Mater.*, 2021, **20**, 859–868.
19 J.-H. Kong, N.-S. Jang, S.-H. Kim and J.-M. Kim, *Carbon*, 2014, **77**, 199–207.
20 R. Lin, H.-J. Kim, S. Achavananthadith, Z. Xiong, J. K. W. Lee, Y. L. Kong and J. S. Ho, *Nat. Commun.*, 2022, **13**, 2190.

21 S. Liu, D. S. Shah and R. Kramer-Bottiglio, *Nat. Mater.*, 2021, **20**, 851–858.
22 W. A. D. M. Jayathilaka, K. Qi, Y. Qin, A. Chinnappan, W. Serrano García, B. Chinnappan, H. Wang, J. He, S. Cui, S. Thomas and S. Ramakrishna, *Adv. Mater.*, 2019, **31**, 1805921.
23 M. Amjadi, K.-U. Kyung, I. Park and M. Sitti, *Adv. Funct. Mater.*, 2015, **26**, 1678–1698.
24 M. Lerond, A. Subramanian, W. G. Skene and F. Cicoira, *Front. Phys.*, 2021, **9**, 708914.
25 T. L. Andrew, L. Zhang, N. Cheng, M. Baima, J. J. Kim, L. Allison and S. Hoxie, *Acc. Chem. Res.*, 2018, **51**, 850–859.
26 L. Kayser and D. Lipomi, *Adv. Mater.*, 2019, **31**, 1806133.
27 P. Yadav and A. Patra, *Polym. Chem.*, 2020, **11**, 7275–7292.
28 M. J. Donahue, A. Sanchez-Sanchez, S. Inal, J. Qu, R. M. Owens, D. Mecerreyes, G. G. Malliaras and D. C. Martin, *Mater. Sci. Eng., R*, 2020, **140**, 100546.
29 X. Fan, W. Nie, H. Tsai, N. Wang, H. Huang, Y. Cheng, R. Wen, M. Liujia, F. Yan and Y. Xia, *Adv. Sci.*, 2019, **6**, 1900813.
30 Y. Guo, M. T. Otley, M. Li, X. Zhang, S. K. Sinha, G. M. Treich and G. A. Sotzing, *ACS Appl. Mater. Interfaces*, 2016, **8**, 26998–27005.
31 S. Darabi, M. Hummel, S. Rantasalo, M. Rissanen, I. Öberg Månsson, H. Hilke, B. Hwang, M. Skrifvars, M. M. Hamedi, H. Sixta, A. Lund and C. Müller, *ACS Appl. Mater. Interfaces*, 2020, **12**, 56403–56412.
32 D. Evans, *Chem. Commun.*, 2022, **58**, 4553–4560.
33 J. Rivnay, S. Inal, B. A. Collins, M. Sessolo, E. Stavrinidou, X. Strakosas, C. Tassone, D. M. Delongchamp and G. G. Malliaras, *Nat. Commun.*, 2016, **7**, 11287.
34 Y. Ding, M. Invernale and G. Sotzing, *ACS Appl. Mater. Interfaces*, 2010, **2**, 1588–1593.
35 C. Yeon, G. Kim, J. Lim and S. Yun, *RSC Adv.*, 2016, **7**, 5888–5897.
36 S. Sinha, Y. S. Noh, N. Reljin, G. Treich, S. Hajeb, Y. Guo, K. Chon and G. Sotzing, *ACS Appl. Mater. Interfaces*, 2017, **9**, 37524–37528.
37 H. Jo, C.-W. Park, S. An, A. Aldalbahi, M. El-Newehy, S. Park, A. Yarin and S. Yoon, *NPG Asia Mater.*, 2022, **14**, 23.
38 S. Maity, S. Datta, M. Mishra, S. Banerjee, S. Das and K. Chatterjee, *Polym. Adv. Technol.*, 2021, **32**, 1409–1427.
39 M. Clevenger, H. Kim, H. W. Song, K. S. No and S. Lee, *Sci. Adv.*, 2021, **7**, abj8958.
40 M. Tadesse, D. A. Mengistie, Y. Chen, L. Wang, M. C. Loghin and V. Nierstrasz, *J. Mater. Sci.*, 2019, **54**, 9591–9602.
41 O. Ala, B. Hu, D. Li, C.-L. Yang, P. Calvert and Q. Fan, *ACS Appl. Mater. Interfaces*, 2017, **9**, 29038–29046.
42 L. Xu, J. xu, Y. Yang, X. Mao, X. He, Y. Wenyao, Y. Zhao and Y. Zhou, *J. Mater. Sci. Mater. Electron.*, 2018, **29**, 2322–2330.
43 G. Fenoy, O. Azzaroni, W. Knoll and W. Marmisollé, *Chemosensors*, 2021, **9**, 212.
44 L. Jimison, A. Hama, X. Strakosas, V. Armel, D. Khodagholy, E. Ismailova, G. Malliaras, B. Winther-Jensen and R. Owens, *J. Mater. Chem.*, 2012, **22**, 19498–19505.
45 V. Karagkiozaki, P. Karagiannidis, M. Gioti, P. Kavatzikidou, D. Georgiou, E. Georgaraki and S. Logothetidis, *Biochim. Biophys. Acta, Gen. Subj.*, 2013, **1830**, 4294–4304.
46 M. Fabretto, M. Müller, K. Zuber and P. Murphy, *Macromol. Rapid Commun.*, 2009, **30**, 1846–1851.
47 C. Yi, L. Zhang, R. Hu, S. Chuang, J. Zheng and X. Gong, *J. Mater. Chem. A*, 2016, **4**, 12730–12738.
48 R. Yewale, P. Damlin, M. Salomäki and C. Kvarnstrom, *Mater. Today Commun.*, 2020, **25**, 101398.
49 Y. Jia, X. Li, F. Jiang, C. Li, T. Wang, Q. Jiang, J. Hou and J. Xu, *J. Polym. Sci., Part B: Polym. Phys.*, 2017, **55**, 1738–1744.
50 W. W. Chiu, J. Travaš-Sejdić, R. P. Cooney and G. A. Bowmaker, *J. Raman Spectrosc.*, 2006, **37**, 1354–1361.
51 S. Garreau, G. Louarn, J. P. Buisson, G. Froyer and S. Lefrant, *Macromolecules*, 1999, **32**, 6807–6812.
52 I. Zozoulenko, J. F. Franco-Gonzalez, V. Gueskine, A. Mehandzhiyski, M. Modarresi, N. Rolland and K. Tybrandt, *Macromolecules*, 2021, **54**, 5915–5934.
53 Y. Sun, H. Li, R. Hou, M. Diao, Y. Liang, Z. Huang, M. G. Humphrey and C. Zhang, *ACS Appl. Mater. Interfaces*, 2020, **12**, 48982–48990.
54 A. Rousti, T. Maji, C. Drew, J. Kumar and D. Christodouleas, *Appl. Mater. Today*, 2021, **25**, 101180.
55 X. Zheng, Q. Hu and W. Nie, *Nanoscale*, 2021, **13**, 1832–1841.
56 L. Allison and T. Andrew, *Adv. Mater. Technol.*, 2019, **4**, 1800615.
57 N. Cheng, L. Zhang, J. Joon Kim and T. L. Andrew, *J. Mater. Chem. C*, 2017, **5**, 5787–5796.
58 Y. H. Jung, B. Park, J. Kim and T.-I. Kim, *Adv. Mater.*, 2019, **31**, 1803637.
59 B. Nie, R. Huang, T. Yao, Y. Zhang, Y. Miao, C. Liu, J. Liu and X. Chen, *Adv. Funct. Mater.*, 2019, **29**, 1808786.

